Designing Constricted Microchannels To Selectively Entrap Soft Particles

Guangdong Zhu, Alexander Alexeev, and Anna C. Balazs*

Chemical Engineering Department, University of Pittsburgh, Pittsburgh, Pennsylvania 15261

Received March 19, 2007; Revised Manuscript Received May 11, 2007

ABSTRACT: The entrapment of micron-sized particles in microscopic pores is beneficial for the efficient functioning of filtration systems and microfluidic devices for analyzing individual biological cells. To optimize the performance of these systems, it is important to isolate factors that regulate the passage of particles through micron-sized constrictions. Using computational modeling, we investigate the fluid-driven motion of compliant particles through constrictions, which are formed by pillars that extend from the top and bottom walls of a microchannel. The particles are modeled as fluid-filled capsules that have elastic shells and simulate biological cells or polymeric microcapsules. The separation between the pillars is ∼10% larger than the diameter of the undeformed capsules. We introduce an attractive interaction between the capsules and the tops of the pillars and vary the elasticity of both the capsules and pillars. Surprisingly, we find that this simple system shows a selectivity toward capsules of intermediate stiffness. Softer capsules are readily deformed by the viscous forces and do not experience the attractive interaction with the pillars, while stiffer capsules cannot deform to maximize the favorable contact with the "sticky" tops. By varying the elasticity of the pillars, we can tailor the range of capsules that become stuck between the pillars. The findings provide guidelines for designing filtration systems and yield insight into the factors that drive particles to block microscopic channels.

Introduction

Understanding the fluid-driven motion of micron-scale particles through pores and constrictions is vitally important for designing a variety of effective filtration systems, including those for purifying water.[1] Additionally, researchers have recently begun to fabricate microfluidic devices to trap and analyze individual biological cells.[2−4] To formulate specifications for these systems, one must know how the physical characteristics of both the particles and the constrictions affect the efficiency of the devices in selectively removing or trapping the desired particles. Of particular interest is understanding how the compliance of the particles affects their movement through narrow passages. There are a number of diseases that alter the mechanical properties of cells and the flow of cells in microfabricated channels can be utilized to detect the presence of such diseases.[3−5] For example, assays in microfluidic channels have shown that while the elastic, uninfected cells could pass through the constrictions, the highly infected, more rigid cells did not traverse these pores and ultimately blocked the system.[4] Studies probing the effect of a particle's stiffness on its movement through capillaries can provide useful guidelines for tailoring the design of effective screening devices.

In addition to screening cells, microfluidic systems that encompass narrow channels could be used to analyze the quality of synthesized micron-scale particles, such as polymeric microcapsules, as well as segregate the preferred species. There is growing interest in exploiting polymeric microcapsules, which encompass a polymer shell and a fluid-filled interior, in a variety of technological applications, from the food, personal care, and pharmaceutical industries to inkless paper.[6] In this context, it would be valuable to create a quick assay that could isolate the species with the desired mechanical properties. For example, one could design systems that trap only those capsules with the specified range of moduli, allowing the nondesired species to escape. A subsequent imposed flow (at, for example, a higher shear rate) could then be used to remove the entrapped microcapasules.

Isolating the factors that lead to entrapment of soft particles within constrictions is rather complicated; it is not simply a matter of the ratio of the particle size to the height of the pore.[7] In particular, viscous forces from the surrounding fluid will distort the size of soft particles, and the extent of this distortion depends on the particle's compliance.[8−13] Additionally, the compliance of the confining walls can have an important effect on the ability of the particles to pass through pores. To the best of our knowledge, few studies have examined how synergistic interactions between deformable particles and compliant walls contribute to particles being trapped within microscopic pores or constrictions. This, however, is an important issue since the walls microfluidic devices, as well as various filters, are commonly fashioned from relatively soft polymeric materials. Thus, studies that take into account the mechanical properties of the pores can enhance our understanding of the factors that lead to particles being entrapped within the microscopic cavities.

In this paper, we use a hybrid computational model[8−13] to investigate how the compliance of both the particles and the confining walls affect the ability of the particles to become trapped within a pore or constriction. In particular, we use our "LBM/LSM" approach,[8−13] which integrates the lattice Boltzmann model (LBM) for hydrodynamics[14] and the lattice spring model (LSM) for the micromechanics of elastic solids.[15−17] Using this approach, we specifically focus on fluid-filled elastic shells (see Figure 1) since they serve as simple models for both biological cells[18−22] and synthetic microcapsules.[8] Researchers have carried out computational studies of the dynamic interactions between cells (modeled as fluid-filled shells) and substrates.[18−20] What is unique to both our previous studies[8−11] and the present investigation is that we examine how the substrate's compliance affects the capsules movement.

In this study, we concentrate on the fluid-driven motion of capsules through a single two-dimensional (2d) constriction; an

* Corresponding author. E-mail: balazs1@engr.pitt.edu.

10.1021/ma0706632 CCC: $37.00
Published on Web 06/14/2007

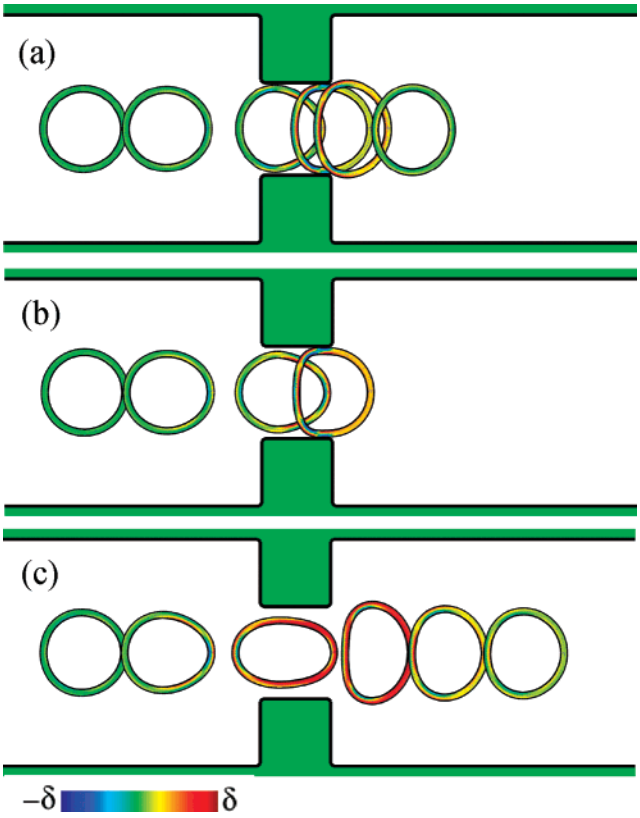

Figure 1. Snapshots of fluid-driven capsules moving (from left to right) through a microchannel that encompasses a constriction, which is formed from rigid adhesive pillars. The three capsules differ in their values of stiffness (as expressed by *Ca*): (a) $Ca = 8.4 \times 10^{-4}$, (b) $Ca = 1.7 \times 10^{-3}$, and (c) $Ca = 6.8 \times 10^{-3}$. The adhesion strength is $\Lambda = 385$. The colors in the capsule's shell indicate the local strain field (see scale bar where $\delta = 0.02$).

image of the entire system is shown in Figure 1. The constriction is formed by pillars that lie in registry and extend from the top and bottom walls of a fluid-filled microchannel; the initial interpillar gap is ∼10% larger than the diameter of the undeformed capsules. Additionally, we introduce an attractive interaction between the capsules and the tops of the pillars (surfaces facing into the channel) to tailor the "responsiveness" of the constriction to the capsules.

We note that different types of boundary element methods have been developed to model capsule motion in straight and constricted tubes.[21,22] In addition to the investigations cited above on cells entering and leaving constrictions, experimental studies have probed the motion and deformation of synthetic capsules (a fluid enclosed in a thin polymeric membrane) in narrow tubes for different capillary numbers and capsule sizes.[23] There are two features of our work that make it distinct from previous studies. First, we vary the attractive interaction between the capsules and the adhesive pillars. These studies can reveal how the combination of chemical heterogeneities and physical asperities affect the flow behavior. Beyond providing guidelines for sorting capsules by their mechanical properties, the findings also yield design criteria for trapping cells that have the same mechanical properties but differ in their adhesive interactions with the pillars. Alterations in the adhesive properties of cells are also a hallmark of various diseases, and thus, such studies can help expand the repertoire of assays that could be carried out in microfabricated channels.

Second, we vary the compliance of the pillars. As will be seen below, by considering the flexibility of these posts, we can provide guidelines for tailoring the range of particles that are trapped in microfluidic devices. These guidelines could be implemented in experimental setups since both the adhesive and mechanical properties of the polymers used in microfluidic devices can be altered through soft lithographic techniques.

Finally, we emphasize that we are considering constrictions that are slightly larger than the diameter of the undeformed capsule. Hence, we are exploring phenomena where the blockage occurs not simply due to geometrical constraints (as, for example, in ref 4), but rather through a subtle interplay between mechanical and adhesive forces.

Below, we first briefly describe the LBM/LSM technique and then detail how the system parameters affect the movement of the microcapsules in the microchannels.

Methodology

In our studies, a compliant two-dimensional capsule is driven through a 2d microchannel by a pressure gradient in the lateral direction. To capture the complex dynamic interactions between the fluids and surfaces in this system, we use our "LBM/LSM" approach,[8−13] which integrates the lattice Boltzmann model (LBM) for hydrodynamics[14] and the lattice spring model (LSM) for the micromechanics of elastic solids.[15−17] The method has been detailed in previous papers,[8,9] and thus, we present just a brief description here. Before the Conclusions section, we also note how the simulation parameters used herein compare with physical values.

The LBM is an efficient solver for the Navier−Stokes equations.[14] In the LSM,[15−17] a compliant material is described by a network of harmonic "springs", which interconnect nearest- and next-nearest neighboring lattice nodes. To capture the dynamics of the solid material, we numerically integrate Newton's equation of motion, $\mathbf{F}(\mathbf{r}_i) = M(\partial^2\mathbf{r}_i/\partial t^2)$, where M is the mass of the node located at position $\mathbf{r}_i$ and $\mathbf{F}$ is the total force acting on the node. The fluid and solid systems interact through the appropriate boundary conditions.[8−13] In particular, the velocities of lattice spring nodes situated at the solid−fluid interface are transmitted to the surrounding fluids. In turn, these LSM nodes experience forces due to the fluid pressure and viscous stresses at the interface; this force is applied as a load to the neighboring LSM nodes. The total force on the LSM nodes also includes an adhesion force (see further below).

To model the bounding walls of the microchannel and the pillars, we use a simple square lattice. For the rigid walls, the LSM nodes are taken to be immobile and the spacing between nodes is equal to 1.5 (measured in LB units). For the flexible pillars, we specify the spring constants k for the eight springs that connect the nearest- and next-nearest neighbor LSM nodes. By varying k, we can modify the Young's modulus of the channel walls and the pillars, $E_S = 5k/2\Delta x$, where Δx is the lattice spacing in the LSM.

The capsule's thin, elastic shell is modeled by a cylindrically symmetric lattice of springs, consisting of three concentric layers of $N = 100$ nodes that lie a distance Δx_c apart. We again use eight springs to connect nearest- and next-nearest neighbor nodes. The equilibrium length for each lattice spring is $\Delta x_c \approx 1.5$, and the shell thickness is $h_c \approx 3.0$ (in LB units).

The following Morse potential describes the capsule−surface interactions: $\phi(r) = \epsilon(1 - \exp[-(r - r_0)/\kappa])^2$, where ϵ and κ characterize the respective strength and range of the interaction potential. The parameter r is the distance between a pair of LSM nodes, where one node lies on the shell's outer surface and the other lies at the substrate−fluid interface, and r_0 is the equilibrium distance. In our simulations, we fix $\kappa = 1$ and $r_0 = 1.8$. (The value of $r_0 = 1.8$ provides a sufficient distance between

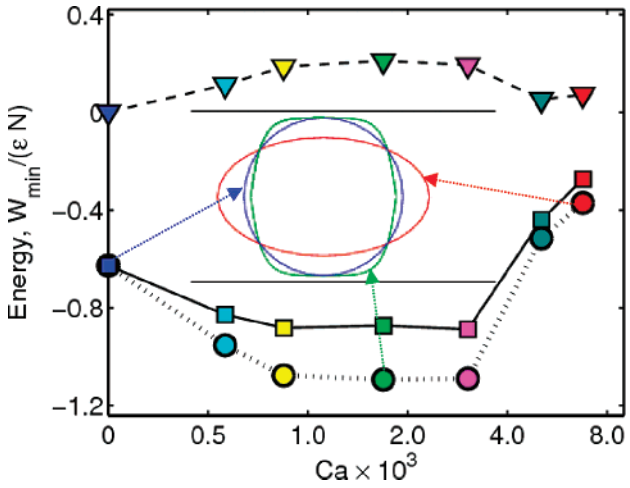

Figure 2. Minimum potential energies, W_{min} (normalized by ϵN here), of a capsule as a function of *Ca* (points are indicated by squares). Also drawn are the two components that contribute to W_{min}: the elastic component of W_{min} (points indicated by triangles) and the adhesive component of W_{min} (points indicated by circles). The curves in the inset reveal the shapes of the capsules inside the constriction; the color of the lines indicates the corresponding value of *Ca* (marked in the same color on the plot).

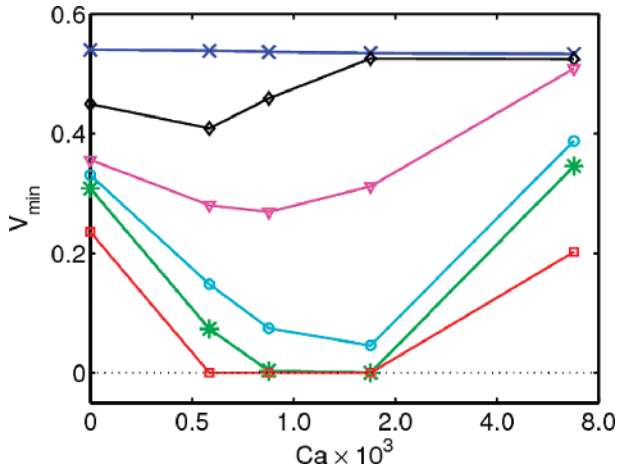

Figure 3. Minimum capsule velocity, V_{min} , as a function of *Ca* for different values of the adhesion strength, Λ. From top to bottom: $\Lambda = 0$ (crosses), $\Lambda = 118$ (diamonds), $\Lambda = 237$ (triangles), $\Lambda = 355$ (circles), $\Lambda = 385$ (stars), and $\Lambda = 473$ (squares).

the capsule and substrate that we capture the lubrication flow between these two bounding surfaces.)

To ensure that the capsules do not penetrate the channel's walls, we impose a repulsive interaction between the capsule and these surfaces.[24] In particular, for the repulsive part of the Morse potential ($r < r_0$), we fix $\epsilon = 1/60$, while we set $\epsilon = 0$ for $r > r_0$, where the potential is attractive. To probe the effect of adhesion on the capsules' dynamics, we introduce an attractive interaction between the capsules and the tops of the pillars by setting $\epsilon = \epsilon_a > 0$ for $r > r_0$.

Various potential interactions can and have been used to model the adhesion of a capsule to a substrate;[25,26] what is important for capturing physically realistic behavior[25] is an interaction potential that includes a strongly repulsive short-range interaction and a weakly attractive long-range interaction. Numerically, the Morse potential is particularly suitable because it has a nearly harmonic repulsive part, which minimizes numerical problems when coupled with the LSM. We note that the specific form of potential may depend on particular experimental conditions.[27] Nevertheless, our general findings could be obtained with other potentials, as long as the shape of this potential is qualitatively similar to the one chosen here.

We perform our simulations in the limit of low Reynolds number, where the effect of inertia can be neglected relative to the viscous forces. The respective fluid density and shear viscosity for both the host and encapsulated fluids are $\rho = 1$ and $\mu = 1/6$. To characterize the relative importance of viscous forces vs the elastic response of the capsule shell, we define a capillary number $\mathrm{Ca} = \mu U_0/(E_c h_c)$. Here, E_c is the Young's modulus of the shell, h_c is the shell thickness, and $U_0 = H^2/12\mu\nabla_x P$ is the average fluid velocity in a straight channel of height H due to a pressure gradient $\nabla_x P$. We also introduce the dimensionless parameter $\Lambda = \epsilon_a N/(\mu U_0 \kappa^2)$, which represents the relative importance of the adhesive strength to the viscous drag force acting on a capsule. Here, $N = 100$ is the number of attractive nodes on the capsule's outer surface. To characterize the pillar stiffness, we introduce $\theta = 2\nabla_x P L l_y^3/E_S l_x^3$, which gives the relative deflection of the pillar due to the applied pressure gradient $\nabla_x P$. In these studies, we model capsules that are tens of microns in size, focusing on the following range of parameters: $Ca \sim 10^{-4}-10^{-3}$, $\Lambda \sim 10^2$, and $\theta \sim 0-10^{-2}$. At the end of the Results and Discussion section, we describe how these simulation values compare to parameters that characterize physical systems.

Before performing the calculations described below, we first validated our approach by carrying out a series of numerical simulations for the steady-state motion of rigid particles moving inside a straight channel. Previously, Sugihara−Seki[28] used a finite element approach to obtain solutions for a circular cylinder in channel flow, which corresponds to our two-dimensional simulations. To compare our findings with these prior results, we selected a channel height of $H = 54$ (in LB units) and length of $L = 8H$; the channel walls are assumed to be rigid. The diameter of the rigid capsule is varied from $0.5H$ to $0.9H$. The flow is driven by a fixed pressure gradient $\nabla_x P = 3.33 \times 10^{-6}$ along the channel, placing the system in the low Reynolds number regime. The particle is placed midway between the channel walls, and we the calculated the steady-state velocity of the particle for different ratios of the particle diameter to channel height. We obtained quantitative agreement with the Sugihara−Seki[28] calculations; that is, our values lie within 0.5% of the values reported by the latter authors.

We also compared our numerical 2d results for compliant capsules with findings obtained by Queguiner and Barthes-Biesel,[21] who used a boundary integral method to examine the axisymmetric motion of elastic capsules in rigid, cylindrical channels in three dimensions. While it is difficult to make a direct comparison between the 2d and 3d results, we nonetheless find that our results for relatively large, deformable capsules qualitatively reproduce their observed power-law relationship between the capsule's relative velocity and capillary number.

In the simulations reported herein, the outer diameter of the undeformed capsule is given by the parameter D and is set to $D = 50$ (in LB units). The height of the channel is $H = 2.6D$, and its length (in the x-direction) is $L = 12.9D$. The thickness of the channel walls is $0.3D$. The length and height of the pillars are $l_x = 0.88D$ and $l_y = 0.76D$, respectively, and the interpillar gap is $h = 1.08D$. Periodic boundary conditions are applied at both ends of the simulation box. The capsule is initially placed at a position along the centerline of the channel, sufficiently far from the constriction to allow the capsule to reach a nearly constant velocity due to the pressure gradient $\nabla_x P = 10^{-6}$ (in LB units). To check that the lattice resolution is sufficient to capture the lubrication forces in the film between the capsule

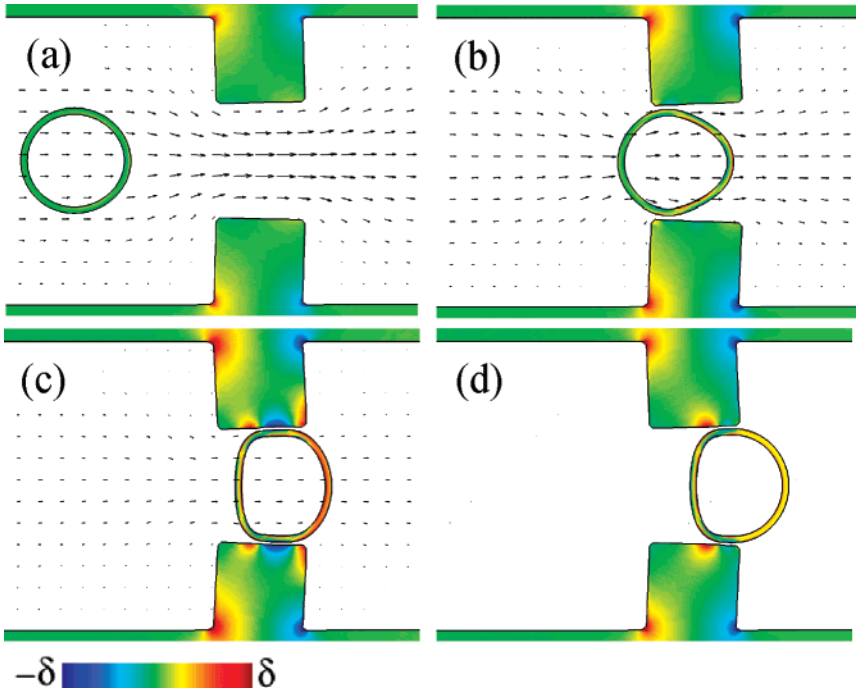

Figure 4. Snapshots of a capsule ($Ca = 1.4 \times 10^{-3}$) moving in a channel with adhesive elastic pillars ($\theta = 0.006$). The images in (a)−(d) are for successively increasing intervals of time. Arrows show the velocity in the fluids; the direction of the arrows indicates the direction of the fluid flow, and the size of the arrow indicates the magnitude of the velocity. The magnitude of the local strain inside capsule's shell and the pillars is indicated by the in color bar, where $\delta = 0.02$. The adhesion strength is $\Lambda = 385$. Note that the capsule in (d) the capsule is trapped by the posts, and thus, the fluid velocity is equal to zero.

and wall, we doubled the lattice resolution of the system and found a difference of less than 0.5% between the cases of different lattice resolution.

Results and Discussion

Rigid Pillars. We start by considering the movement of elastic capsules through channels with rigid pillars. The snapshots in Figure 1 reveal the dynamic behavior of three capsules with different stiffness; for this study, we fix $\Lambda = 385$. The colors within the capsule indicate the strain within the elastic material. Surprisingly, we find that although the stiffer ($Ca = 8.4 \times 10^{-4}$) and softer ($Ca = 6.8 \times 10^{-3}$) capsules are able to pass through the constriction, the capsule with an intermediate value of stiffness ($Ca = 1.7 \times 10^{-3}$) is firmly trapped by the adhesive pillars at the downstream exit of the constriction. Since the gap between the pillars is larger than the undeformed capsule diameter, the trapping of the capsules is due to the adhesive interaction.

To explore this behavior, we calculate the energy, W, that is associated with the capsule−pillar adhesion and the elastic deformation of the capsule's shell. The adhesive interaction energy is measured directly from the Morse potential acting between the walls and the capsule; the energy associated with the elastic deformation is simply calculated from the strain within the spring network of our LSM. Note that the attractive adhesive interaction acts to reduce the total energy, while the elastic deformation increases W. In Figure 2, we plot the minimal values of the energy, W_{min}, as a function capsule stiffness, which is expressed via Ca. (The capsule's structure far from the constriction serves as the reference point for the energy calculation.) Most notably, W_{min} has a minimum at approximately $Ca \sim 10^{-3}$; we correlate the decrease in W_{min} for capsules with intermediate values of Ca to an increase in contact area between the capsule's shell and the tops of the pillars (see inset in Figure 2). For a given magnitude of the adhesion strength, the softer, more deformable capsules exhibit a larger contact area with the pillar's "sticky" tops. When the modulus of the shell is sufficiently small, however, the capsules undergo significant deformation due to the viscous forces arising from the surrounding fluid. As a result, these highly compliant capsules remain far away from the pillar tops (see Figure 1c) so that the adhesive interaction is too weak to affect the motion of these soft particles.

We find that the lower the value of W_{min}, the larger the magnitude of the applied force (pressure gradient) required to drive the capsule through the constriction. Alternatively, for a fixed pressure drop, modifying the interaction strength Λ allows us to tailor the range of capsules that will be trapped. To illustrate this point, we calculated the minimum velocity V_{min} attained by different capsules during their motion along the channel; V_{min} equals zero when a capsule is firmly trapped by the adhesive pillars. Figure 3 shows V_{min} vs Ca for a range of Λ. As expected, an increase in the adhesion strength reduces the minimal velocity of the capsules; the effect is most pronounced for intermediate values of Ca, i.e., $6 \times 10^{-4} < Ca < 2 \times 10^{-3}$. (Note that for nonadhesive pillars there is little variation in V_{min}, which in this case is close to the velocity of the capsules away from for the constriction.) When the adhesion is sufficiently strong that $\Lambda \geq 385$, V_{min} goes to zero, indicating that certain capsules are trapped by the pillars. The range of Ca for which the capsules are trapped increases with increasing Λ.

Elastic Pillars. To gain greater control over the range of capsules that could be trapped, we consider channels with elastic walls and pillars. The pillars are sufficiently soft that they can be readily deformed due to interactions with the adhesive particles and the flow, as shown in Figures 4 and 5. In particular, Figure 4 shows the trapping of a compliant capsule ($Ca = 1.4 \times 10^{-3}$) by pillars with $\theta = 0.006$. Our findings on the behavior of the capsules are summarized in the map in Figure 6, which

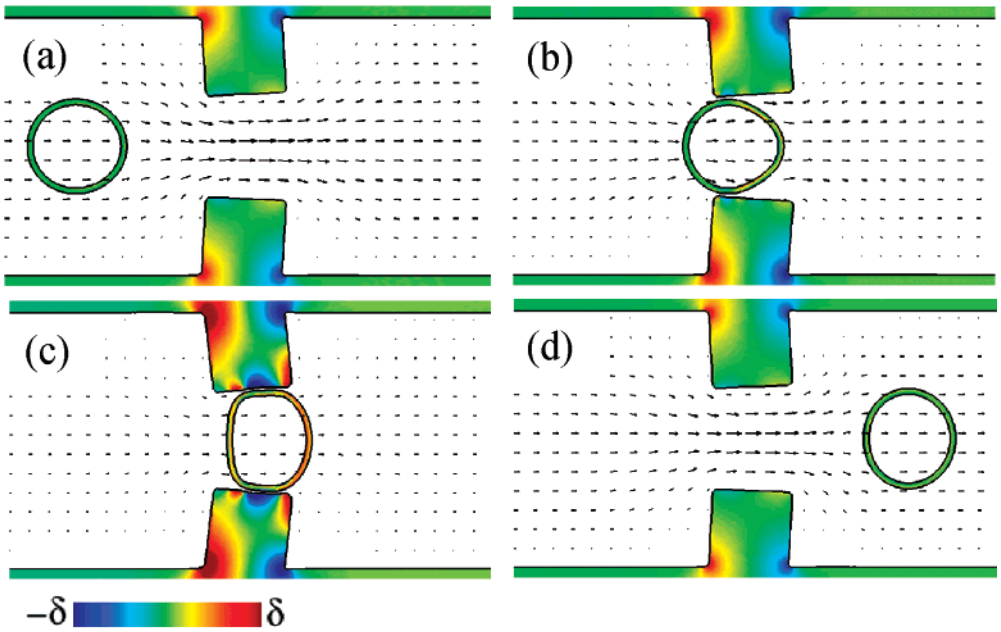

Figure 5. Snapshots of a capsule ($Ca = 1.4 \times 10^{-3}$) moving in a channel with softer adhesive elastic pillars ($\theta = 0.012$) than those in Figure 4. The other parameters are the same as those in Figure 4.

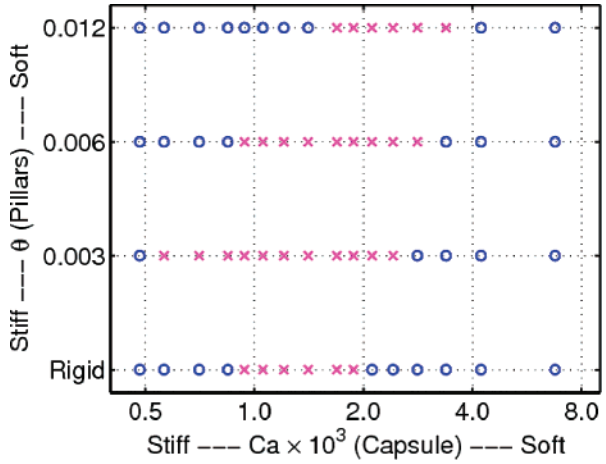

Figure 6. Phase map showing the behavior of capsules of different stiffness moving through a channel with adhesive pillars of different stiffness. The crosses indicate parameters for which the capsules are trapped by the pillars, while the circles mark the situations where the capsules pass through the constriction without being trapped. The adhesion strength is $\Lambda = 385$.

is plotted in terms of Ca for the capsules and the pillar deflection, θ. The circles indicate conditions for which the capsules pass through the constriction, while the crosses mark the situations where the capsules are firmly trapped by the pillars. Figure 6 clearly reveals that the range of Ca for which the capsules are trapped depends on the pillar stiffness. Specifically, pillars with $\theta = 0.006$ trap somewhat stiffer capsules than the rigid pillars because these compliant posts can adjust to the shape of capsules and, therefore, increase the contact area. This, in turn, increases the magnitude of the energy drop due to the adhesion between the pillars and capsules.

For softer pillars, however, the bending of the entire pillars by the viscous flow (see Figure 5) becomes relatively important and eventually dominates in defining the range of capsules that can be trapped. The changes in the geometry of the softer pillars reduce the gap at the constriction's entrance and increase this gap at the outlet, where the capsules are normally trapped. As a result of the enhanced gap at the outlet, relatively stiff capsules can more easily escape through the constriction (see Figure 5). On the other hand, softer capsules are trapped more easily, as they are affected more strongly by the adhesion at the narrow inlet and are able to deform to maximize contact with the distorted outlet.

Comparison of Simulation Parameters with Experimental Values. As noted in the Introduction, we propose that such topologically patterned surfaces could be harnessed to segregate synthetic microcapsules as well as certain biological cells. In this section, we compare the range of values of our dimensionless parameters, Ca and Λ, to comparable experimental values. We first consider an example of polyelectrolyte microcapsules[29] that are propelled by an imposed flow in an aqueous solution whose viscosity is $\mu \approx 10^{-3}$ kg/(s m) and density is $\rho \approx 10^3$ kg/m^3. Typical velocities in microfluidic devices are on the order of 1 cm/s, and typical channel heights are hundreds of microns.[30] Using experimentally realistic values of the membrane thickness h, which are on the order of tens of nanometers for a 10 μm capsule,[31] and the stiffness of the microcapsule shell Eh, which are on the order of $10^{-3}-1$ N/m,[32] we obtain capillary numbers of $Ca \sim 10^{-5}-10^{-2}$, which is in the range considered in the simulations.

The results are also appropriate for considering the fluid-driven motion of leukocytes. Leukocytes have a cytoskeleton that serves to maintain the spherical shape of the cell, and these cells have in fact been modeled as fluid-filled elastic shells. In such modeling studies, researchers typically use an effective membrane stiffness that lies in the range 0.01−0.3 N/m,[18,20] which is also within the range of parameters considered for the microcapsules. Thus, for leukocytes with radii on the order of 5 μm in an aqueous solution within a microchannel, one obtains typical values of the capillary number $Ca \sim 10^{-4}-10^{-3}$.

With respect to the adhesion, a polyelectrolyte coating on the substrate can be utilized to produce an adhesive interaction between the microcapsule and the substrate. The total adhesion energy can be estimated to be on the order of $w \sim 10^{-16}-10^{-14}$ J/capsule,[33,34] while the interaction range is roughly $\kappa \sim 10^{-8}-10^{-7}$ m.[35] Recall that we define a dimensionless interaction strength, $\Lambda = \epsilon N/\mu U_0 \kappa^2$; if we set ϵN to be on the order of w, we find that Λ is on the order of 10^3-10^4. For micron-scale

biological particles interacting with substrates, the adhesion energy is in the range of $w \sim 10^{-19}-10^{-15}$ J[26,36,37] and $\kappa \sim 10$ nm;[26,36] these values yield $\Lambda \sim 10^2-10^6$. Thus, the Λ used in our simulations fall within experimentally realistic values.

Finally, we note that recent advances in soft lithography permit the fabrication of mechanically patterned substrates that contain regular arrays of compliant posts.[38] In particular, a thick polymer film with a Young's modulus as low as 10−20 kPa can be patterned by standard lithographic techniques[39] to exhibit such features. To implement our predictions, experimentalists could vary the post ratio (l_y/l_x) in order to set θ to the same values as in the simulations. To show that our θ values correspond to feasible scenarios, we note that our value of $\theta \sim 10^{-2}$ can be realized by choosing the following experimentally realistic parameters: (l_y/l_x) ~ 2 and a pressure drop of ∼10 Pa in a channel that is a millimeter long. The latter two choices yield to a flow rate of ∼1 cm/s, which is typical for microfluidic devices.

Conclusions

In summary, we used the LBM/LSM approach to demonstrate how opposed pillars in microchannels can effectively entrap capsules with specific mechanical properties. In the case of rigid pillars, the interplay between the adhesive and viscous forces determines both the capsule's shape and whether the particle becomes lodged between the pillars. Specifically, very soft capsules are deformed by the viscous forces to such an extent that they do not even come into contact with the adhesive regions. On other extreme, stiff capsules cannot be sufficiently deformed by the adhesive interaction to overcome the force of the imposed flow. Thus, only capsules with specific elasticities can be firmly bound by the adhesive pillars. For a fixed imposed flow, the range of capsules that can be trapped strongly depends on the magnitude of the adhesive strength. We also demonstrated that this range could be adjusted by using soft, elastic pillars. In particular, the mutual responsiveness of the deformable pillars and compliant capsules allowed a range of softer particles to be caught.

The above findings could be harnessed to design multipore filters or membranes, where particles with a particular range of mechanical properties are selectively removed from the system, while particles outside of this range can traverse the narrow passages. In the multipore case, the force acting on a capsule would be lower (because the fluid can escape through the open pores); nonetheless, we expect qualitatively similar results, and the magnitude of the dimensionless parameter Λ obtained herein can provide guidance for tailoring the system to obtain the desired results. Similarly, the above findings should also apply if we consider 3d pillars; here, however, the contact between a capsule and the pillars could be smaller than in 2d, meaning that the force due to adhesion is also lower. Again, the values of Λ obtained here can be used to guide efforts in pinpointing the optimal regime for the 3d behavior.

The results also provide insight into the factors that cause particles to clog microscopic pores or constrictions. Namely, the findings highlight how the compliance of the constrictions contributes to trapping attractive capsules and thus to the blockage of the passageways. This issue is particularly relevant to the flow of cells in blood vessels, and our observations can potentially shed light on additional causes leading to clogging in the circulatory system.

Acknowledgment. The authors gratefully acknowledge financial support from DOE (to A.A.) and ONR (to G.Z.).

References and Notes

(1) Auset, M.; Keller, A. A. *Water Resour. Res.* **2004**, *40*, W03503.
(2) (a) Roman, G. T.; Chen, Y.; Viberg, P.; Culbertson, A. H.; Culbertson, C. T. *Anal. Bioanal. Chem.* **2007**, *387*, 9. (b) Johann, R. M. *Anal. Bioanal. Chem.* **2006**, *385*, 408. (c) Valero, A.; Merino, F.; Wolbers, F.; Luttge, R.; Vermes, I.; Andersson, H.; van der Berg, A. *Lab Chip* **2005**, *5*, 49.
(3) Abkarian, M.; Faivre, M.; Stone, H. A. *Proc. Natl. Acad. Sci. U.S.A.* **2006**, *103*, 538.
(4) Shelby, J. P.; White, J.; Ganesan, K.; Rathod, P. K.; Chiu, D. T. *Proc. Natl. Acad. Sci. U.S.A.* **2003**, *100*, 14618.
(5) Rosenbluth, M. J.; Lam, W. A.; Fletcher, D. A. *Biophys. J.* **2006**, *90*, 2994.
(6) Yow, H. N.; Routh, A. F. *Soft Matter* **2006**, *2*, 940 and references therein.
(7) Wyss, H. M.; Blair, D. L.; Morris, J. F.; Sone, H. A.; Weitz, D. A. *Phys. Rev. E* **2006**, *74*, 061402.
(8) Alexeev, A.; Verberg, R.; Balazs, A. C. *Macromolecules* **2005**, *38*, 10244.
(9) Alexeev, A.; Verberg, R.; Balazs, A. C. *Phys. Rev. Lett.* **2006**, *96*, 148103.
(10) Alexeev, A.; Verberg, R.; Balazs, A. C. *Soft Matter* **2006**, *2*, 499.
(11) Alexeev, A.; Verberg, R.; Balazs, A. C. *Langmuir* **2007**, *23*, 983.
(12) Alexeev, A.; Verberg, R.; Balazs, A. C. *J. Polym. Sci., Part B: Polym. Phys.* **2006**, *44*, 2667.
(13) Smith, K. A.; Alexeev, A.; Verberg, R.; Balazs, A. C. *Langmuir* **2006**, *22*, 6739.
(14) Succi, S. *The Lattice Boltzmann Equation for Fluid Dynamics and Beyond*; Oxford University Press: New York, 2001.
(15) Ladd, A. J. C.; Kinney, J. H. *Physica A* **1997**, *240*, 349.
(16) Ladd, A. J. C.; Kinney, J. H.; Breunig, T. M. *Phys. Rev. E* **1997**, *55*, 3271.
(17) Buxton, G. A.; Care, C. M.; Cleaver, D. J. *Model. Simul. Mater. Sci. Eng.* **2001**, *9*, 485.
(18) (a) Dong, C.; Cao, J.; Struble, E. J.; Lipowsky, H. H. *Ann. Biomed. Eng.* **1999**, *27*, 298. (b) Jadhav, S.; Eggleton, C. D.; Konstantopoulos, K. *Biophys. J.* **2005**, *88*, 96 and references therein.
(19) Marella, S. V.; Udaykumar, H. S. *Phys. Fluids* **2004**, *16*, 244.
(20) (a) Krasik, E. F.; Hammer, D. A. *Biophys. J.* **2004**, *87*, 2919. (b) King, M. R.; Hammer, D. A. *Proc. Natl. Acad. Sci. U.S.A.* **2001**, *98*, 14919. (c) Khismatullin, D. B.; Truskey, G. A. *Microvasc. Res.* **2004**, *68*, 188. (d) Hodges, R. S; Jensen, O. E. *J. Fluid Mech.* **2002**, *460*, 381.
(21) Queguiner, C.; Barthes-Biesel, D. *J. Fluid Mech.* **1997**, *348*, 349.
(22) (a) Pozrikidis, C. *Phys. Fluids* **2005**, *17*, 031503 (b) Pozrikidis, C. *Ann. Biomed. Eng.* **2005**, *33*, 165.
(23) Risso, F.; Colle-Paillot, F.; Zagzoule, M. *J. Fluid Mech.* **2006**, *547*, 149 and references therein.
(24) It is in fact the repulsive part of the potential that prevents the capsule from penetrating the walls. The LBM alone does not automatically keep the capsules from overlapping with the substrate.
(25) Sukumaran, S.; Seifert, U. *Phys. Rev. E* **2001**, *64*, 011916.
(26) (a) Cantat, I.; Misbah, C. *Phys. Rev. Lett.* **1999**, *83*, 880. (b) Cantat, I.; Misbah, C. *Phys. Rev. Lett.* **1999**, *83*, 235.
(27) Lipowsky, R.; Sackmann, E. *Structure and Dynamics of Membranes, Handbook of Biological Physics*; Elsevier Science: Amsterdam, 1995; Vols. 1A and 1B.
(28) Sugihara-Seki, M. *J. Fluid Mech.* **1993**, *257*, 575.
(29) See for example: (a) Gao, C. Y.; Leporatti, S.; Moya, S.; Donath, E.; Möhwald, H. *Langmuir* **2001**, *17*, 3491. (b) Lulevich, V. V.; Radtchenko, I. L.; Sukhorukov, G. B.; Vinogradova, O. I. *Macromolecules* **2003**, *36*, 2832. (c) Fery, A.; Dubreuil, F.; Mohwald, H. *New J. Phys.* **2004**, *6*, 18. (d) Vinogradova, O. I. *J. Phys.: Condens. Matter* **2004**, *16*, R1105. (e) Peyratout, C. S.; Dahne, L. *Angew. Chem., Int. Ed.* **2004**, *43*, 3762.
(30) Stone, H. A.; Stroock, A. D.; Ajdari, A. *Ann. Rev. Fluid Mech.* **2004**, *36*, 381.
(31) Dubreuil, F.; Elsner, N.; Fery, A. *Eur. Phys. J. E* **2003**, *12*, 215.
(32) Elsner, N.; Kozlovskaya, V.; Sukhishvili, S. A.; Fery, A. *Soft Matter* **2006**, *2*, 966.
(33) Nolte, M.; Fery, A. *Langmuir* **2004**, *20*, 2995.
(34) Liu, K. K.; Chan, V.; Zhang, Z. *Med. Biol. Eng. Comput.* **2002**, *40*, 491.
(35) Bosio, V.; Dubreuil, F.; Bogdanovic, G.; Fery, A. *Colloids Surf., A* **2004**, *243*, 147.
(36) Leckband, D.; Israelachvili, J. *Q. Rev. Biophys.* **2001**, *34*, 105.
(37) Zhang, X. H.; Chen, A.; De Leon, D.; Li, H.; Nori, E.; Moy, V. T.; Goliogorsky, M. S. *Am. J. Physiol.: Heart Circ. Physiol.* **2004**, *286*, H359.
(38) Chen, C. S.; Jiang, X.; Whitesides, G. M. *MRS Bull.* **2005**, *30*, 194.
(39) Schwarz, U. S.; Balaban, N. Q.; Riveline, D.; Bershadsky, A.; Geiger, B.; Safran, S. A. *Biophys. J.* **2002**, *83*, 1380.

MA0706632